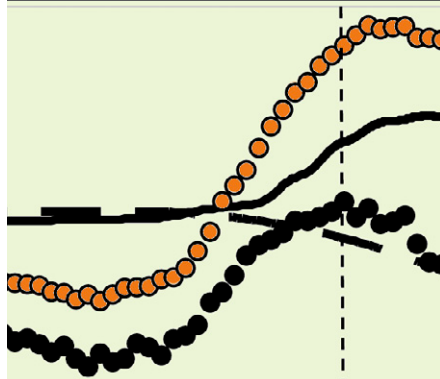**Original Research**

S. Assouline*
K. Narkis
S. W. Tyler
I. Lunati
M. B. Parlange
J. S. Selker

Two dielectric methods (operating at 70 MHz and 1 GHz) were applied to monitor water content profiles in covered and uncovered buckets. Positive correlations were found between temperature and water content in the 5- to 10-cm depth, and these were reproduced by simulating the temperature effect on the soil liquid water content dynamics with HYDRUS-1D.

S. Assouline and K. Narkis, Institute of Soil, Water and Environmental Sciences, ARO, The Volcani Center, Bet Dagan, Israel; S.W. Tyler, Dep. of Geological Sciences and Engineering, Univ. of Nevada, Reno, NV; I. Lunati, Institute of Geophysics, Univ. of Lausanne, Lausanne, Switzerland; M.B. Parlange, School of Architecture, Civil and Environmental Engineering, Ecole Polytechnique Federale de Lausanne (EPFL), Lausanne, Switzerland; and J.S. Selker, Dep. of Biological and Ecological Engineering, Oregon State Univ., Corvallis, OR. *Corresponding author (vwshmuel@agri.gov.il).

On the Diurnal Soil Water Content Dynamics during Evaporation using Dielectric Methods

The water content dynamics in the upper soil surface during evaporation is a key element in land–atmosphere exchanges. Previous experimental studies have suggested that the soil water content increases at the depth of 5 to 15 cm below the soil surface during evaporation, while the layer in the immediate vicinity of the soil surface is drying. In this study, the dynamics of water content profiles exposed to solar radiative forcing was monitored at a high temporal resolution using dielectric methods both in the presence and absence of evaporation. A 4-d comparison of reported moisture content in coarse sand in covered and uncovered buckets using a commercial dielectric-based probe (70 MHz ECH$_2$O-5TE, Decagon Devices, Pullman, WA) and the standard 1-GHz time domain reflectometry method. Both sensors reported a positive correlation between temperature and water content in the 5- to 10-cm depth, most pronounced in the morning during heating and in the afternoon during cooling. Such positive correlation might have a physical origin induced by evaporation at the surface and redistribution due to liquid water fluxes resulting from the temperature-gradient dynamics within the sand profile at those depths. Our experimental data suggest that the combined effect of surface evaporation and temperature-gradient dynamics should be considered to analyze experimental soil water profiles. Additional effects related to the frequency of operation and to protocols for temperature compensation of the dielectric sensors may also affect the probes' response during large temperature changes.

Abbreviations: TDR, time domain reflectometry.

An accurate description of water content dynamics at the soil surface is crucial in understanding and modeling land–atmosphere interactions. Water content dynamics in the vicinity of the soil surface are affected by the diurnal cycle of atmospheric forcing through solar radiation, wind speed, air temperature and humidity, and surface properties. The expected characteristic diurnal course of surface water content during evaporation is a decrease soon after sunrise until sunset and stabilization or a slight rise at night due to redistribution via capillary rise, perhaps augmented by vapor condensation if the soil surface is exposed to a cold night sky. This trend has been observed in gravimetric water content data for the upper 1.0-cm soil layer (Rose, 1968; Jackson, 1973).

Other measurements obtained by dielectric sensors installed at 3- and 10-cm depths indicated a diurnal course that was opposite to that expected (Verhoef et al., 2006), i.e., apparent soil water content at those depths increased from sunrise until noon and declined until sunset, showing a positive correlation with soil temperature, T. Attempts to correct the sensor response for temperature effects were inconclusive (Verhoef et al., 2006). Cahill and Parlange (1998) also measured atypical diurnal oscillations using time domain reflectometry (TDR). Or and Wraith (2000) suggested that these fluctuations could be explained, in part, in terms of liberation of bound water to the surface of the clay fraction of the soil (Wraith and Or, 1999; Or and Wraith, 1999), whereas Cahill and Parlange (1998, 2000) brought attention to the possible role of vapor movement due to air advection on the atypical dynamics of the measured diurnal soil volumetric water content, θ. Parlange et al. (1998) suggested that the expansion and contraction of the soil air resulting from the diurnal heating and cooling of the soil surface might be the cause to the convective transport of water vapor.

To understand diurnal θ dynamics during evaporation, nondestructive monitoring of the water content at different depths and at relatively high frequency (at subhourly resolution) is required. Electromagnetic methods exploit the difference between the dielectric permittivity of water ($\varepsilon_w \sim 80$), soil particles ($\varepsilon_s \sim 2$–9), and air ($\varepsilon_a \sim 1$), thus allowing θ to be estimated and offering the ability to log data automatically (Topp et al., 1980; Wang and Schmugge,

1980; Friedman, 1998; Jones et al., 2002, Robinson et al., 2003). The accuracy of the electromagnetic method is affected by a large range of factors, however, including soil type, clay and organic matter contents, particle shape, temperature, salinity, phase configuration, and interfacial polarization (Wraith and Or, 1999; Jones and Friedman, 2000; Robinson and Friedman, 2001; Jones and Or, 2002; Robinson et al., 2003). Temperature fluctuations are known to have significant effects on the dielectric properties of the medium and on the response of the sensor. The temperature dependence of the dielectric permittivity of water, for instance, is well described to be linear through the empirical relationship $\varepsilon_w = 88 - 0.35T$, for water temperature T varying between 5 and 40°C (Weast, 1986). The relative importance of the temperature-induced errors is influenced by the frequency used by the measuring device (Chen and Or, 2006a,b). Sensors operating at frequencies lower than 100 MHz could be significantly affected by temperature due to Maxwell–Wagner polarization effects (Chen and Or, 2006b), and soil moisture measurements can be biased even with carefully calibrated sensors. Seyfried and Grant (2007) quantified the temperature effects on the dielectric permittivity of oven-dry and saturated soils using the Hydra Probe soil water sensor (Stevens Water Monitoring Systems, Portland, OR) operating at 50 MHz. They found that for temperatures ranging from 5 to 45°C, a maximum apparent water content change of ±0.028 cm^3 cm^{-3} was observed for the saturated soil samples while oven-dry samples were insensitive to temperature changes, which suggests that the temperature effects largely result from the water. Bogena et al. (2007) reported that the ECH$_2$O-EC5 sensor, which uses the same circuitry as the ECH$_2$O-5TE (Decagon Devices, Pullman, WA), generally showed an increase in measured soil water content with increasing temperature. The maximum error in soil water content due to temperature effects on the sensor circuitry varied between −1.1% at 5°C to 1.8% at 40°C.

Temperature is also known to affect the soil hydraulic properties (Gardner, 1955; Philip and de Vries, 1957; Nimmo and Miller, 1986; Hopmans and Dane, 1986; Grant and Salehzadeh, 1996). Grant and Bachmann (2002), in a review of the four most intuitive mechanisms that could explain the observed effect of temperature on capillary pressure, and consequently, on water content in soils (these being expansion of water, expansion of entrapped air, surface tension, and contact angle), came to the conclusion that all failed to satisfactorily describe the experimental data.

In this study, water content profiles in sand buckets exposed to solar radiative forcing were monitored at a high temporal resolution using dielectric methods both in the presence and absence of evaporation. The objectives of this study were to: (i) investigate the diurnal θ dynamics during evaporation; and (ii) analyze the possible errors in dielectric-based soil moisture measurements due to temperature fluctuations. The apparent θ dynamics were monitored by means of two different dielectric sensors operating at two different frequencies: the ECH$_2$O-5TE operating at 70 MHz and a TDR cable tester connected to a custom three-rod probe operating nominally at 1 GHz.

◆ Methodology

In the experiment, coarse, air-dried sand (with an approximately normal distribution of grain sizes from 250 to 710 μm, with a mean value of 500 μm) was packed in two buckets (40-cm diameter by 25-cm height) to a bulk density of 1.60 ± 0.03 g cm^{-3}. During the packing, one ECH$_2$O-5TE probe and one three-rod probe (15.0-cm-long, 2.80-mm-diameter rods and 15.0-mm rod spacing) were installed horizontally (with blades sideways) in each bucket at depths of 5.0, 10.0, and 15.0 cm below the surface; the sensors were located with depth in a helical pattern to avoid mutual interference.

The ECH$_2$O-5TE sensors are reported to operate at 70 MHz and utilize three 5.2-cm-long prongs that provide a three-probe electrical array for bulk electrical conductivity, a dielectric permittivity sensor for θ estimates, and a thermistor for temperature measurement. Each set of three sensors was connected to an Em50 datalogger (Decagon Devices, Pullman, WA), and θ and T data were collected and stored every 15 min. The 5TE probe infers the bulk dielectric permittivity, ε_b, from the capacitance of the surrounding medium. A 70-MHz signal is supplied to charge the prongs, the charge being a function of the soil dielectric permittivity and volumetric water content. A microprocessor measures that charge and outputs a raw value from the probe. The 5TE sensor is factory calibrated, and the raw output corresponds to $50\varepsilon_b$.

The performance of the six sensors used was tested in a preliminary experiment where all the sensors measured similar conditions and the resulting sensor-to-sensor variability was relatively low: estimated as 3.5% for the water content and 2% for the temperature. Furthermore, the reliability of the ECH$_2$O-5TE thermistor was assessed in an independent heating–cooling experiment by comparison with reference data obtained with thermocouples: the transient temperature measured by the thermistors was identical to those from the thermocouples. Detailed testing of sensor-to-sensor variability of the 5TE can be found in Rosenbaum et al. (2010).

Using a Tektronics 1502 metallic cable tester with the TDR probes is often reported as a 1-GHz measurement. It should be noted that because it uses a step change in voltage as its interrogating signal, it is actually a signal that has all frequencies represented, from sub-megahertz up to about 2.0 GHz. However, the effective frequency is definitely within the gigahertz range rather than megahertz (Robinson et al., 2003). The six three-rod TDR probes were connected to the Tektronics 1502 metallic cable tester via a 16-channel multiplexer (Dynamax, Houston, TX) and the waveforms sampled every 15 min. The electrical length calibration of the probes was performed in distilled water at room temperature (~21°C). The waveform travel time analysis was performed using the WinTDR software (Or et al., 2003).

The calibration curve for coarse sand suggested by Robinson et al. (2005) was used to transform the soil dielectric permittivity
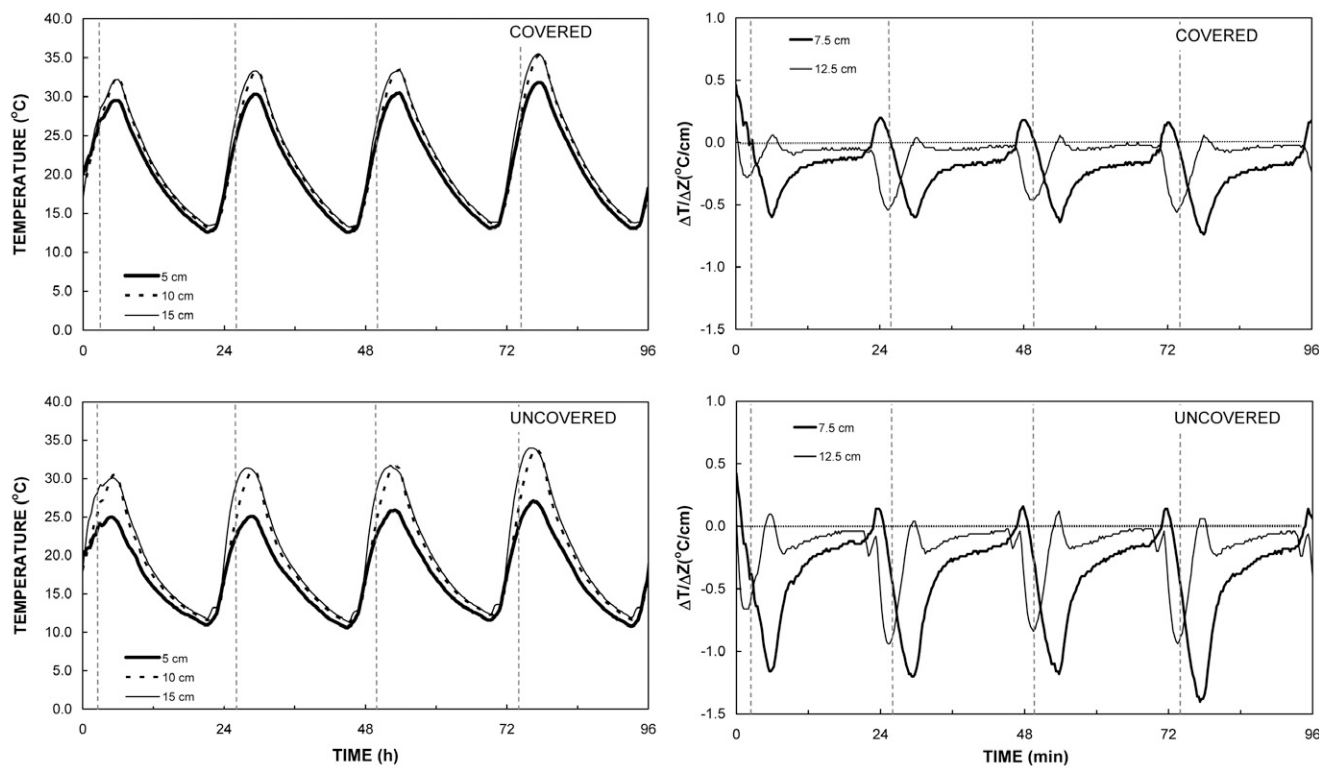
Fig. 1. Measured temperatures (left) and estimated temperature gradients with depth, $\Delta T/\Delta Z$, (right) at the different depths and for the covered and uncovered surfaces. The vertical dashed lines indicate 1200 h daily.

measurements into volumetric water content, θ, estimates for both sensor types. These estimates of θ were corrected for the temperature effect on the permittivity of the water, assuming the Maxwell–Garnett mixing equation (Robinson et al., 2005).

The sand surface was wetted evenly using a sprayer with distilled water, and the amount of water added to the buckets corresponded to an initial mean water content of 0.26 ± 0.01 m³ m⁻³. The use of distilled water and leached sand allow us to assume that the contribution of changes in electrical conductivity to the observed error in θ should be very small.

One bucket was covered with a transparent polyethylene sheet to prevent evaporation, while the other bucket was left uncovered. The uninsulated buckets were exposed in an open area from 19 to 23 Nov. 2009. The experiment took place at the A.R.O. campus in Bet-Dagan (32°0′ N, 34°48′ E), Israel. During the measurement period, days were clear and sunny, and no rain was measured. The observed net solar radiation, air temperature, and relative humidity during the experiment are presented in the Appendix (Fig. A1).

◆ Results
Temperature Measurements
Sand temperature, T, was measured at all depths, Z, by the built-in thermistor of the ECH$_2$O-5TE probes in both the covered and

uncovered buckets (Fig. 1). The temperature gradient was estimated from the discrete T measurements according to

$$\frac{\Delta T}{\Delta Z}\left(i+\frac{1}{2}\right)=\frac{T_i - T_{i+1}}{\left|Z_i - Z_{i+1}\right|} \qquad [1]$$

where the depth index $i = 1$ corresponds to $Z = 5$ cm, and $i = 3$ corresponds to $Z = 15$ cm.

In the covered bucket, diurnal soil temperature T followed the expected quasi-sinusoidal temporal distribution, peaking at 1200 h (Fig. 1, upper left panel). The temperature variation at the vicinity of the surface (5.0-cm depth) ranged from a minimum close to 15°C slightly before sunrise to a maximum around 30°C (for the covered sand) in the early afternoon. The maximum difference between the surface and deeper soil layers (10 and 15 cm) was ~3°C. This relatively small difference and the relatively short phase shift in the maxima and minima of T with depth can be explained by the fact that the buckets did not exchange heat only at the sand surface but also radially through the bucket walls. Therefore, the response in terms of $T(Z)$ is different from the behavior that would have been simulated by a one-dimensional sand column model of heat transport. Regarding the temperature gradients (Fig. 1, upper right panel), the buildup of a positive gradient (decreasing T with depth) in the morning hours, with a maximum before 1200 h, is depicted for the 5- to 10-cm layer, while the buildup of a negative gradient occurred in the 10- to 15-cm layer.
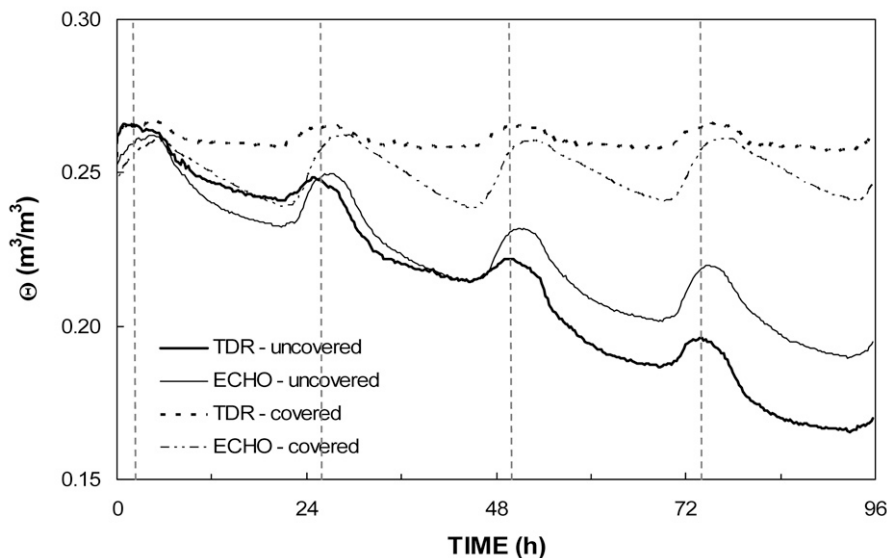
Fig. 2. Computed weighted mean water content (Θ) for the time domain reflectometry (TDR) probes and ECH$_2$O-5TE probes for the covered and uncovered sand buckets. The vertical dashed lines indicate 1200 h daily.

When evaporation occurred (the uncovered case), the maximal temperature close to the surface was reduced to 25°C (cooling effect) (Fig. 1, lower left panel), resulting in a larger difference within the whole profile. This increased the amplitudes of the temperature gradients (Fig. 1, lower right panel) without affecting the general trends shown in the covered case where evaporation was prevented.

Volumetric Water Content Measurements

The initial water content distribution with depth in the buckets was consistent with the hydrostatic conditions. The mean water content, Θ, was approximated as the weighted mean of θ_i at the depth Z_i. The weighting factors corresponded to the relative thickness of the corresponding sand layer:

$$\Theta = \frac{\sum_{i=1}^{3} \left(d_i \theta_i \right)}{\sum_{i=1}^{3} d_i} \qquad [2]$$

where d_i is the thickness of the sand layer represented by the measured water content θ_i. The dynamics of Θ during the experiment is depicted in Fig. 2. By design, the covered buckets should show a constant total water content, but the computed mean water content fluctuated in phase with the diurnal temperature (Fig. 2). It appears that the readings of the ECH$_2$O-5TE and the TDR probes are still both sensitive to temperature even after the applied correction for a temperature effect on the permittivity of the water assuming the Maxwell–Garnett mixing equation (Robinson et al., 2005), and that the Θ values estimated by the two sensor types are similar only late in the afternoon.

The computed mean water content in the uncovered buckets decreased steadily during the experiment and followed the expected evaporation pattern, with superimposed daily fluctuations, as in the covered case, due to temperature dynamics. Both sensor types captured the main trend in Θ but a difference between the ECH$_2$O-5TE and the TDR build after the second day, with the TDR indicating lower Θ values. The estimated water content at the end of the experiment, based on weighing the uncovered bucket at the beginning and end of the experiment, was 0.14 ± 0.01 m^3 m^{-3}, suggesting that the TDR sensors are more accurate that the ECHO-5TE ones.

The dynamics of θ as a function of depth monitored by the two sensor types are distinct (Fig. 3). For the covered buckets, the TDR sensors (Fig. 3a) depicted the hydrostatic distribution of θ with depth, and showed the superimposed fluctuation in phase with temperature dynamics. The ECH$_2$O-5TE sensors (Fig. 3b) depicted a less gradual change in θ with depth, as would be expected from a hydrostatic profile wherein the magnitudes of the readings taken at the 10-cm depth are close to those taken at the 5-cm depth but the time dependence of the 10-cm measurements are more closely akin to the 15-cm observations. The temperature impact is noticeable in both sensors and at all depths, being more marked at the 5-cm depth (Fig. 3a and 3b).

When evaporation took place (Fig. 3c and 3d), θ decreased, as would be expected, at the shallower and intermediate depths (5 and 10 cm), while it remained practically constant at the deeper sensor (15 cm). Here, too, water content apparently peaked at 1200 h, and it seems that the stronger effect corresponded to the intermediate probe at the 10-cm depth. Because the overall bucket measurements showed that the actual total water content decreased monotonically, this apparent gain of mass may be attributed to instrument error. Interestingly, it can be seen in Fig. 3c that $\theta(t)$ for $Z = 5$ cm is concave while $\theta(t)$ for $Z = 10$ cm is convex, indicating that the water demand for evaporation was provided in the early stages by the upper sand layer and later on by the deeper layer.

The water content data of the last day of the experiment were expressed vs. the corresponding measured temperature T for the covered and uncovered cases (Fig. 4). The resulting $\theta(T)$ relationships depicted practically linear relationships. For the deeper TDR probes (Fig. 4a and 4c), where the sand was very humid, the slope of these relationships is practically 0, independent of the surface condition: the applied correction for temperature was appropriate and compensated satisfactorily for temperature effect on the permittivity of the water. For the shallower TDR probe, however, a positive slope was measured in the covered case (Fig. 4a), indicating that the correction for temperature was not sufficient
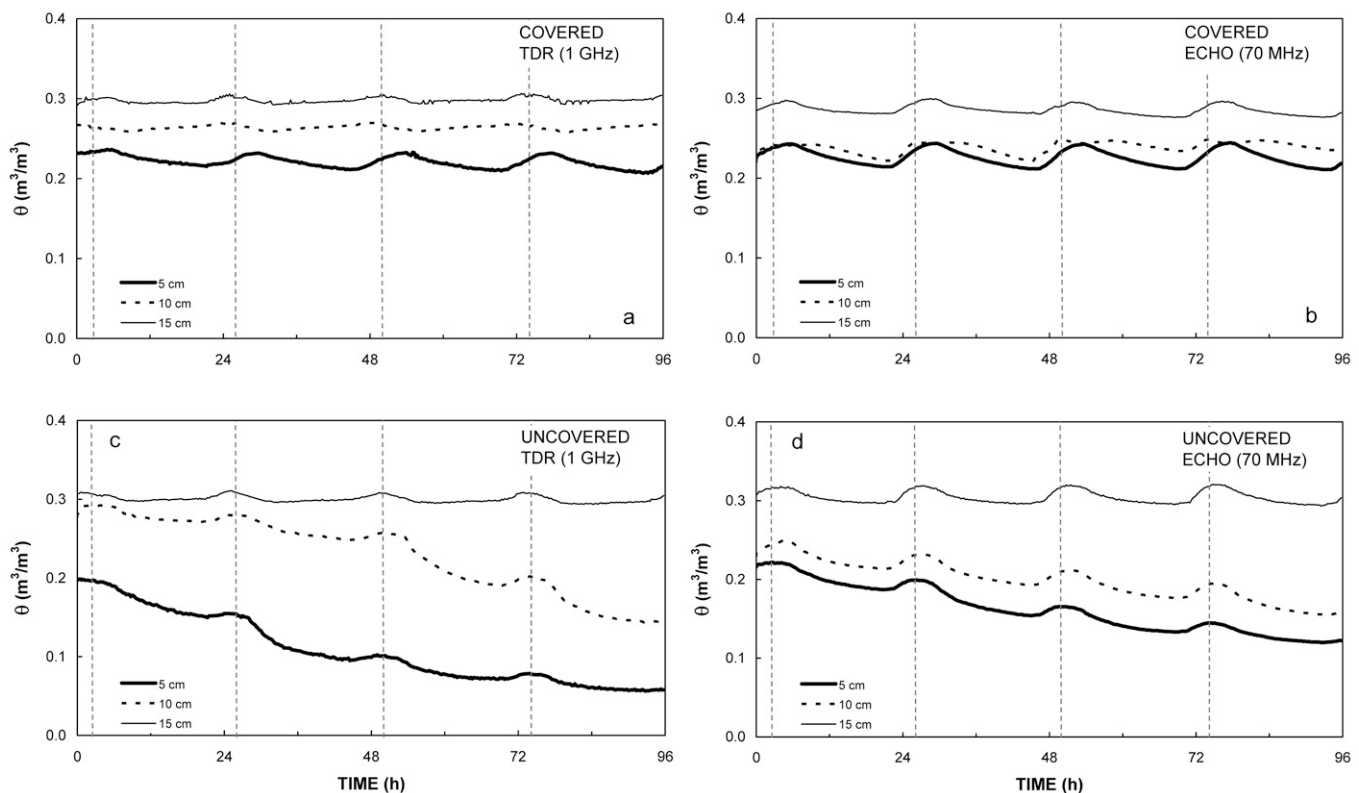
Fig. 3. Measured sand water content (θ) by means of (a and c) time domain reflectometry (TDR) probes and (b and d) ECH₂O-5TE probes at the different depths and for the (a and b) covered and (c and d) uncovered sand buckets. The vertical dashed lines indicate 1200 h daily.

and suggesting that other factors have to be considered. When evaporation occurred, the positive slope is noticeable mainly in the afternoon, when cooling took place while evaporation continued. This positive slope is steeper at the 10-cm depth (Fig. 4c), suggesting that processes within the sand profile might be the reason for such "atypical" behavior.

When data from the ECH₂O-5TE probes are considered (Fig. 4b and 4d), a positive slope in θ(T) is noticeable at all depths and independent of the surface condition. Such positive slope indicates that compensation for the effect of temperature on the water permittivity was not enough for that specific sensor type and that additional causes still induced a positive correlation between temperature and water content.

◆ Discussion

The apparent diurnal θ dynamics measured by dielectric sensors during evaporation (Cahill and Parlange, 1998; Or and Wraith, 2000; Verhoef et al., 2006) generated a debate about the nature and causes of such an "atypical" behavior. The primary difficulty in explaining the observed trend of positive temperature–soil water content correlation stems from the fact that it is well established that water dielectric permittivity decreases with increasing temperature (Weast, 1986; Pepin et al., 1995). This implies that an increase in T results in a decrease in the soil dielectric permittivity. This leads to a

misestimation of θ when a calibration with no temperature compensation is used. In the following, we evaluate to what extent different factors and mechanisms might be at the origin of the observed sensor response and could contribute to explaining the experimental results.

Effect of Bound Water

The physical model of Or and Wraith (1999) has shown that, depending on the water content and the surface area of the specific soil under interest, the dielectric permittivity of the medium measured by TDR can either increase or decrease with increasing temperature due to the opposing temperature response of the bulk and bound soil water dielectric constants. Therefore, coarse sand, with very low surface area, was chosen for this experiment to minimize the effect of bound water, and we assume that it was negligible in this experiment.

Operating Frequency and Maxwell–Wagner Polarization

The two types of sensors used in this study operate at different frequencies: the TDR probes effectively measure at approximately 1 GHz whereas the ECH₂O-5TE probes operate at 70 MHz. The effects of frequency have been long recognized (e.g., Campbell, 1990), and studied with respect to changes in T by Chen and Or (2006a,b). The nature of soils as mixtures of constituents with different dielectric constants and separated by numerous interfaces gives rise to Maxwell–Wagner polarization. Interfacial processes are dominant at lower frequencies
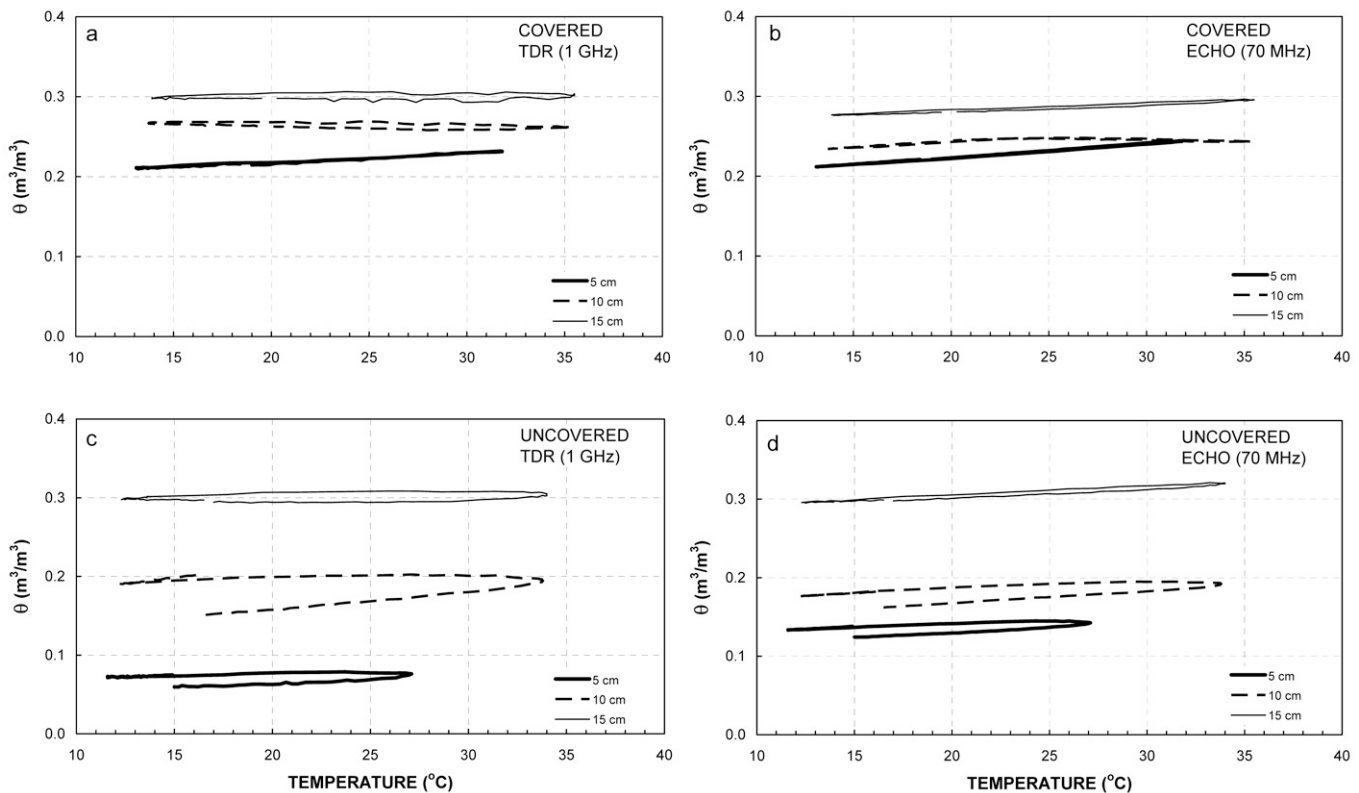
Fig. 4. The relationships between water content and temperature, $\theta(T)$, for (a and c) the time domain reflectometry probes and (b and d) ECH$_2$O-5TE probes at the different depths and for the (a and b) covered and (c and d) uncovered sand buckets for the last day of the experiment.

and can significantly affect the θ estimates when temperature changes are significant. Direct measurements using a network analyzer and model calculations (Chen and Or, 2006b) have shown that below the frequency of 100 MHz, the measured dielectric permittivity increases with increasing temperature, while it decreases with increasing temperature above this threshold, as is observed for free water (Weast, 1986; Pepin et al., 1995). If Maxwell–Wagner polarization is a relevant mechanism for ECH$_2$O probe measurements, a clear positive correlation between temperature and water content is expected, as was observed (Fig. 4b and 4d). Thermal effects on the Maxwell–Wagner polarization mechanism could thus explain, at least in part, the atypical response of the ECH$_2$O-5TE probes. Indeed, the ratio of surface area to water volume increases with decreasing water content, which might favor the effects of Maxwell–Wagner polarization over the effects of temperature on bulk water dielectric permittivity at lower water contents.

The TDR data are expected to be unaffected by Maxwell–Wagner polarization effects because the sensors operate far above the 100-MHz crossover frequency shaping the thermal effect on interfacial polarization (Robinson et al., 2003). Figures 4a and 4c depict no temperature effect on θ after compensation for the effect of T on the water permittivity for the deeper probes. A positive correlation between θ and T was observed on the whole profile (Fig. 2), however, and mostly at soil depths of 5 and 10 cm for this sensor

type also (Fig. 4a and 4c). Therefore, other physical mechanisms have to be at the origin of such positive correlation.

Effect of Temperature on Water Vapor Fluxes

Another possible mechanism for the observed changes in behavior may be the migration of water vapor due to thermal and pressure gradients. The water vapor flux, q_v, can be approximated following de Vries' model (de Vries, 1958):

$$q_v = -\xi D_a \, \eta \, \mathrm{grad}\rho_v \qquad [3]$$

where D_a is the diffusivity of water vapor in still air, ρ_v, is the saturated vapor density at a given temperature, η is the enhancement factor, and ξ is the product of the tortuosity factor times the air-filled porosity, which was defined following Millington and Quirk (1961):

$$\xi = \left(n-\theta\right)^{1.33}\left(1-\frac{\theta}{n}\right)^2 \qquad [4]$$

where θ is the measured water content of the respective layers and n is the total porosity. The diffusivity of water vapor, D_a, was estimated by an expression resulting from a linear fit to the data reported by Gates (1980) (Holsoft Web Design, 2001):

$$D_a = 21.2\times10^{-6}\left(1+0.0071T\right) \qquad [5]$$

where D_a is in square meters per second and T is in degrees Celsius. The enhancement factor, η, was evaluated for the sand (no clay fraction) following Cass et al. (1984):

$$\eta = 9.5 + 3\frac{\theta}{n} \qquad [6]$$

The temperature data for the last day of the experiment were used to estimate the vapor pressure at each depth, e_{si}, assuming water-vapor-saturated air in the pores (Allen et al., 1998):

$$e_{si} = 611.2 \exp\left(\frac{17.502 T_i}{T_i + 240.97}\right) \qquad [7]$$

where T_i is the layer temperature (in °C) and e_{si} is in pascals. The corresponding ρ_{vi} values were estimated according to (Brutsaert, 1982)

$$\rho_{vi} = \frac{0.622\, e_{si}}{R_d\, T_{ai}} \qquad [8]$$

where R_d is the gas constant (287.04 J kg^{-1} K^{-1}) and T_{ai} is the absolute temperature of the soil layer (K). The gradient $d\rho_{vi}/dZ_i$ was computed for the different layers, as in Eq. [1] for dT_i/dZ_i.

The resulting predicted vapor fluxes are depicted in Fig. 5 for covered and uncovered conditions. The trends are basically similar for the covered and uncovered cases but the amplitude of the diurnal variation of the flux is four times larger in the uncovered case, where evaporation occurred. In the morning, from approximately 0900 to 1030 h, negative fluxes (directed downward) were computed for the upper layer (7.5-cm depth) while fluxes in the opposite direction (positive fluxes) were computed for the deeper layer (12.5-cm depth). Therefore, during that period, accumulation of vapor could occur at the 10-cm depth, and a possible condensation of that vapor on the cooler sand could theoretically increase the water content at that depth and partly explain the "atypical" behavior of the sensors. The amount of water added by such a process is very small, however—below the detection level of the sensors. From 1030 h, the vapor fluxes at both depths were positive and directed upward. The flux peaked at 1200 h at the 12.5-cm depth, while it peaked in the afternoon (around 1500 h) at the 7.5-cm depth. Interestingly, at that time, the vapor flux reversed direction at the 12.5-cm depth.

In conclusion, although the direction of the vapor fluxes at the different depths was consistent with the observed changes in θ, their magnitude is insufficient to explain the reported changes. It is interesting to note that the computed vapor fluxes are on the same order of magnitude as the fluxes resulting from the theory of Parlange et al. (1998), where the convective transport of water vapor, not considered here, was addressed.

Effect of Temperature on Liquid Water Fluxes
To investigate the effect of the sand temperature on the liquid water flux, and consequently on θ, numerical simulations were performed with the modified version of HYDRUS-1D that solves the coupled
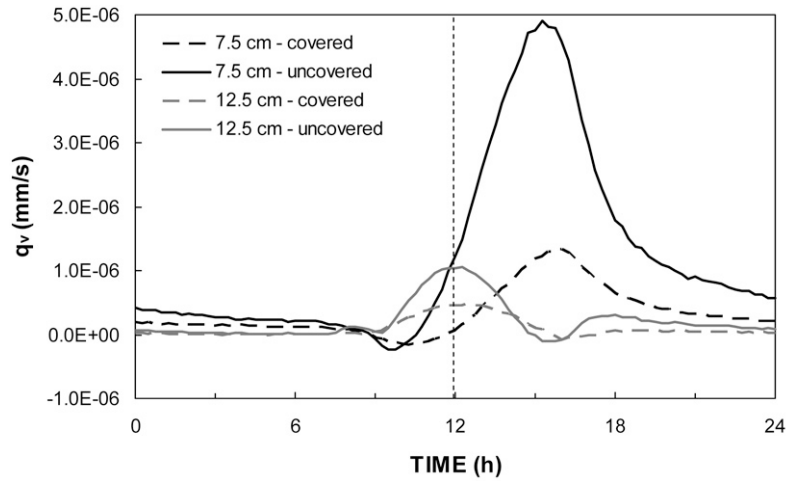

Fig. 5. Estimated diurnal dynamics of the diffusive fluxes of water vapor, q_v, for the different layers of the covered (dashed lines) and uncovered (solid lines) sand buckets. The vertical dashed line indicates 1200 h.

equation governing liquid water and heat transport (Saito et al., 2006). That version accounts also for the effect of temperature on the soil water retention curve using the gain factor suggested by Nimmo and Miller (1986), as well as for the effect of temperature on the water surface tension. These preliminary simulations did not aim to reproduce the experimental data but to give a qualitative estimate of the impact of temperature changes on the liquid water flux as well as the θ dynamics. Indeed, the one-dimensional approximation did not fully correspond to the experimental setup, which allowed for heat exchange through the bucket walls.

The hydraulic and thermal properties of the sand were taken directly from the built-in catalog of soil properties in HYDRUS. The initial conditions corresponding to the hydrostatic θ profile and measured T profile at 000 h were implemented. Temperature values measured at the 5.0-cm depth were assumed as conditions for the temperature at the upper boundary. The covered case was simulated by assuming a no-flux boundary at the surface, while hourly evaporation rates estimated from Fig. 2 were used for the upper boundary of the uncovered case. A no-flux condition was used for the lower boundary in all the cases. A 48-h simulation was performed and compared with an analogous calculation in which the temperature was kept constant with time to highlight the effect of temperature on the simulated liquid flux.

The fractional change in water content, $\Delta\theta/\theta_o = (\theta - \theta_o)/\theta_o$ (θ_o denotes the initial value of θ at 000 h, $t = 0$), during the second day of the simulation is provided in Fig. 6 for the case where temperature effects were neglected (dashed line) and the case where they were accounted for (solid line) for the covered (upper plot) and uncovered (lower plot) cases. For comparison purposes, the corresponding trends measured by the TDR and the ECH$_2$O-5TE probes are also depicted in Fig. 6. Data showing a clear positive correlation between T and θ (Fig. 4), namely, the 5-cm depth
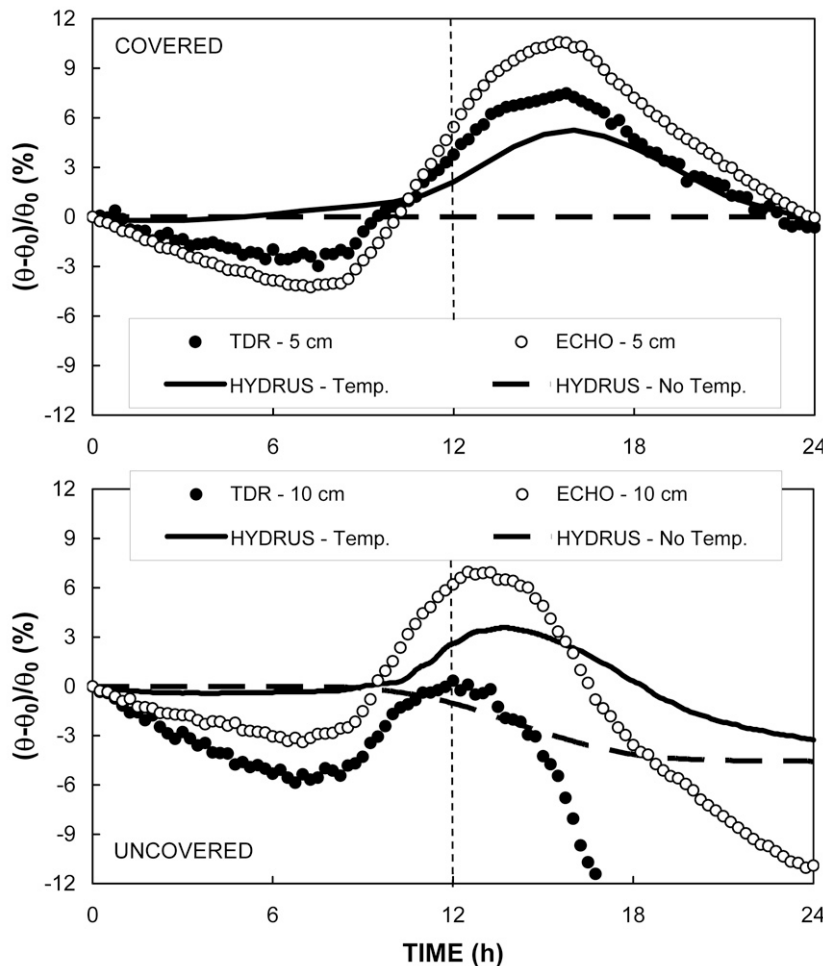
Fig. 6. Diurnal dynamics of the fractional change in water content, $\theta - \theta_o/\theta_o$, for the second day of the simulation when temperature effects are accounted for (solid line) and neglected (dashed line), and the corresponding time domain reflectometry (TDR) and ECH$_2$O-5TE probe data in the covered (upper plot) and uncovered (lower plot) sand buckets. The simulation was performed using the HYDRUS-1D version accounting for heat transport (Saito et al., 2006). The vertical dashed lines indicates 1200 h.

for the covered case and the 10-cm depth for the uncovered case, were chosen to illustrate the measured trends. When temperature effects were neglected, the simulated $\Delta\theta/\theta_o = 0$ in the covered case; it decreased monotonically during the daytime as evaporation took place and remained practically constant in the absence of evaporation at night in the uncovered case (dashed lines in Fig. 6). When temperature effects were accounted for, the simulated water content dynamics during the day reproduced the measured trends: $\Delta\theta/\theta_o$ increased during the morning hours when the sand heated up, peaked shortly after noon, then decreased while evaporation continued but the sand was already beginning to cool off. This result indicates that temperature effects on liquid fluxes and water content dynamics could therefore contribute to explain the observed positive correlation between θ and T measured by the dielectric sensors.

Summary and Conclusions

Various published experimental studies where upward evaporation was induced observed an apparent wetting during the daytime occurring 5 to 15 cm below the surface. Because this behavior was measured by means of dielectric methods, known to be affected by temperature, the possibility of an artifact was considered and debated. In this study, nondestructive dielectric methods were applied to monitor water content profiles at a high temporal resolution (every 15 min) in covered and uncovered buckets to prevent and allow evaporation, respectively. Two different sensors were used: TDR, operating at 1 GHz, and the ECH$_2$O-5TE, operating at 70 MHz.

Both sensors detected a positive correlation between temperature and water content at certain hours of the day, mainly at the 10-cm depth, even though the data were corrected for the decrease in the dielectric permittivity of water with increasing temperature.

This positive correlation between temperature and water content is clearly noticeable and persistent during cooling but also shortly after sunrise when the soil temperature started rising. As TDR operates at 1-GHz frequency and should not be affected by Maxwell–Wagner polarization, this suggests that the observed positive correlation has a physical origin related to flow processes within the sand profile. During cooling, this positive correlation may result from the fact that evaporation continues while the soil temperature begins to decrease in the afternoon. During heating, additional physical processes may be involved. Estimated water vapor diffusive fluxes showed that, for both the covered and the uncovered cases, fluxes in the 10- to 15-cm layer were too small to explain that positive correlation. A preliminary simulation of the temperature effect on the liquid water content dynamics revealed periods of positive correlation between θ and T that corresponded to those observed experimentally. Therefore, the combined effect of surface evaporative fluxes and temperature-gradient dynamics on liquid fluxes should be accounted for when measured data of spatial and temporal distributions of soil water content during evaporation are analyzed.

Additional effects related to the frequency of operation and to protocols for temperature compensation of the probes still play the most significant role in shaping the dielectric sensors' response under experimental conditions. Also, the direct effects of temperature on the ECH$_2$O-5TE circuitry may affect the sensor response, as shown by Bogena et al. (2007) on the

ECH$_2$O-EC5, which uses the same circuit as the 5TE. This suggests that great deference must be used when interpreting subtle changes in the apparent dielectric permittivity under conditions where temperature fluctuations are significant. Alternative nondestructive measurement techniques, such as gamma ray attenuation, may be needed to fully understand these processes.

♦ Appendix

Climatic data during the experiment were monitored at the site. Net radiation was measured by a net radiometer (Q*7.1, REBS, Seattle, WA). Dry- and wet-bulb air temperatures were measured by two aspirating psychrometers, shielded against direct solar radiation. The instruments were positioned 4.0 m above the surface level. The data are presented in Fig. A1.

Fig. A1. Air temperature, relative humidity, and net solar radiation at the experimental site.

References

Allen, R.G., L.S. Pereira, D. Raes, and M. Smith. 1998. Crop evapotranspiration: Guidelines for computing crop water requirements. FAO Irrig. Drain. Pap. 56. FAO, Rome.

Bogena, H.R., J.A. Huisman, C. Oberdörster, and H. Vereecken. 2007. Evaluation of a low-cost soil water content sensor for wireless network applications. J. Hydrol. 344:32–42.

Brutsaert, W. 1982. Evaporation into the atmosphere: Theory, history and applications. D. Reidel Publ. Co., Dordrecht, the Netherlands.

Cahill, A.T., and M.B. Parlange. 1998. On water vapor transport in field soils. Water Resour. Res. 34:731–739.

Cahill, A.T., and M.B. Parlange. 2000. Reply. Water Resour. Res. 36:3107–3110.

Campbell, J.E. 1990. Dielectric properties and influence of conductivity in soils at one to fifty megahertz. Soil Sci. Soc. Am. J. 54:332–341.

Cass, A., G.S. Campbell, and T.L. Jones. 1984. Enhancement of thermal water vapor diffusion in soil. Soil Sci. Soc. Am. J. 48:25–32.

Chen, Y., and D. Or. 2006a. Effects of Maxwell–Wagner polarization on soil complex dielectric permittivity under variable temperature and electrical conductivity. Water Resour. Res. 42:W06424, doi:10.1029/2005WR004590.

Chen, Y., and D. Or. 2006b. Geometrical factors and interfacial processes affecting complex dielectric permittivity of partially saturated porous media. Water Resour. Res. 42:W06423, 10.1029/2005WR004744.

de Vries, D.A. 1958. Simultaneous transfer of heat and moisture in porous media. Eos Trans. Am. Geophys. Union 39:909–916.

Friedman, S.P. 1998. A saturation degree-dependent composite spheres model for describing the effective dielectric constant of unsaturated porous media. Water Resour. Res. 34:2949–2961.

Gardner, R. 1955. Relations of temperature to moisture tension of soils. Soil Sci. 79:257–265.

Gates, D.M. 1980. Biophysical ecology. Springer-Verlag, Berlin.

Grant, S.A., and J. Bachmann. 2002. Effect of temperature on capillary pressure. p. 199–212. In P.A.C. Raats et al. (ed.) Environmental mechanics: Water, mass and energy transfer in the biosphere. Geophys. Monogr. 129. Am. Geophys. Union, Washington, DC.

Grant, S.A., and A. Salehzadeh. 1996. Calculations of temperature effects on wetting coefficients of porous solids and their capillary and wetting WRCs. Water Resour. Res. 32:261–279.

Holsoft Web Design. 2001. Holsoft's physics resources pages. Available at physics.holsoft.nl/physics/physreso.htm (verified 9 July 2010). Holsoft Web Design, the Netherlands.

Hopmans, J.W., and J.H. Dane. 1986. Temperature dependence of soil hydraulic properties. Soil Sci. Soc. Am. J. 50:4–9.

Jackson, R.D. 1973. Diurnal changes in soil water content during drying. p. 37–55. In R.R. Bruce et al. (ed.) Field soil water regime. SSSA Spec. Publ. 5. SSSA, Madison, WI.

Jones, S.B., and S.P. Friedman. 2000. Particle shape effects on the effective permittivity of anisotropic or isotropic media consisting of aligned or randomly oriented ellipsoidal particles. Water Resour. Res. 36:2821–2833.
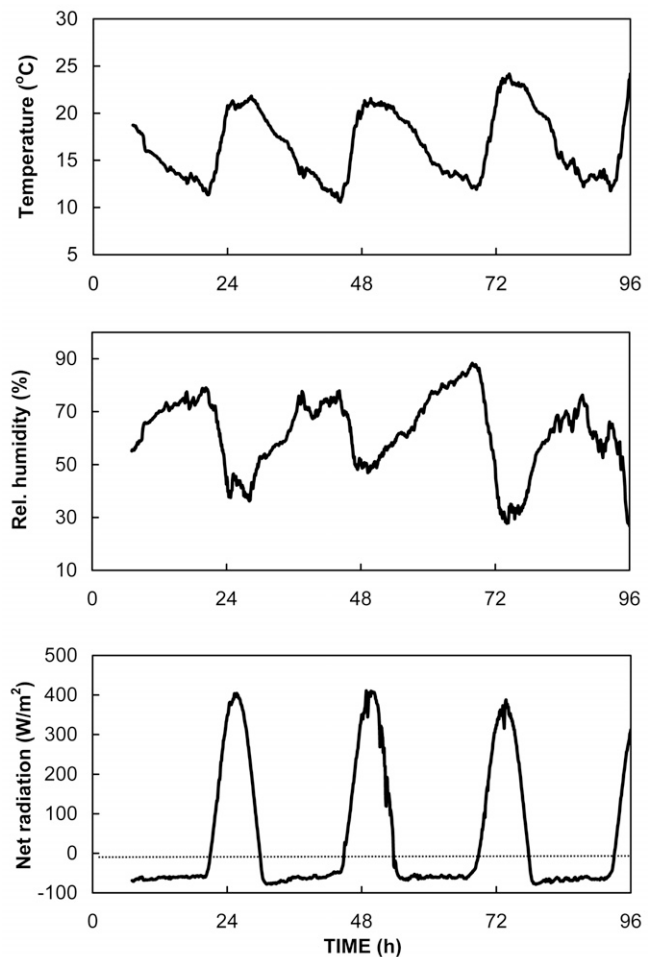
Jones, S.B., and D. Or. 2002. Surface area, geometrical and configuration effects on permittivity of porous media. J. Non-Cryst. Solids 305:247–254.

Jones, S.B., J.M. Wraith, and D. Or. 2002. Time domain reflectometry (TDR) measurement principles and applications. Hydrol. Processes 16:141–153.

Millington, R.J., and J.M. Quirk. 1961. Permeability of porous solids. Trans. Faraday Soc. 57:1200–1207.

Nimmo, J.R., and E.E. Miller. 1986. The temperature dependence of isothermal moisture vs. potential characteristics of soils. Soil Sci. Soc. Am. J. 50:1105–1113.

Or, D., S.B. Jones, J.R. Van Shaar, S. Humphries, and L. Koberstein. 2003. Win-TDR– soil analysis software users guide, Version 6.1. Dep. of Plants, Soil, and Biometeorol., Utah State Univ., Logan.

Or, D., and J.M. Wraith. 1999. Temperature effects on soil bulk dielectric permittivity measured by time domain reflectometry: A physical model. Water Resour. Res. 35:371–383.

Or, D., and J.M. Wraith. 2000. Comment on "On water vapor transport in field soils" by A.T. Cahill and M.B. Parlange. Water Resour. Res. 36:3103–3105.

Parlange, M.B., A.T. Cahill, D.R. Nielsen, J.W. Hopmans, and O. Wendroth. 1998. Review of heat and water movement in field soils. Soil Tillage Res. 47:5–10.

Pepin, S., N.J. Livingston, and W.R. Hook. 1995. Temperature-dependent measurement errors in time domain reflectometry determinations of soil water. Soil Sci. Soc. Am. J. 59:38–43.

Philip, J.R., and D.A. de Vries. 1957. Moisture movement in porous materials under temperature gradients. Trans. Am. Geophys. Union 38:222–232.

Robinson, D.A., and S.P. Friedman. 2001. Effect of particle size distribution on the effective dielectric permittivity of saturated granular media. Water Resour. Res. 37:33–40.

Robinson, D.A., S.B. Jones, J.M. Blonquist, Jr., and S.P. Friedman. 2005. A physically derived water content/permittivity calibration model for coarse-textured, layered soils. Soil Sci. Soc. Am. J. 69:1372–1378.

Robinson, D.A., S.B. Jones, J.M. Wraith, D. Or, and S.P. Friedman. 2003. A review of advances in dielectric and electrical conductivity measurement in soils using time domain reflectometry. Vadose Zone J. 2:444–475.

Rose, C.W. 1968. Water transport in soil with a daily temperature wave: I. Theory and experiment. Aust. J. Soil Res. 6:31–44.

Rosenbaum, U., J.A. Huisman, A. Weuthen, H. Vereecken, and H.R. Bogena. 2010. Sensor-to-sensor variability of the ECH$_2$O EC-5, TE, and 5TE sensors in dielectric liquids. Vadose Zone J. 9:181–186.

Saito, H., J. Šimůnek, and B.P. Mohanty. 2006. Numerical analysis of coupled water, vapor, and heat transport in the vadose zone. Vadose Zone J. 5:784–800.

Seyfried, M.S., and L.E. Grant. 2007. Temperature effects on soil dielectric properties measured at 50 MHz. Vadose Zone J. 6:759–765.

Topp, G.C., J.L. Davis, and A.P. Annan. 1980. Electromagnetic determination of soil water content: Measurement in coaxial transmission lines. Water Resour. Res. 16:574–582.

Verhoef, A., J. Fernández-Gávez, A. Diaz-Espejo, B.E. Main, and M. El-Bishi. 2006. The diurnal course of soil moisture as measured by various dielectric sensors: Effects of soil temperature and the implications for evaporation estimates. J. Hydrol. 321:147–162.

Wang, J.R., and T.J. Schmugge. 1980. An empirical model for the complex dielectric permittivity of soils as a function of water content. IEEE Trans. Geosci. Remote Sens. 18:288–295.

Weast, R.C. (ed.) 1986. CRC handbook of chemistry and physics. 67th ed. CRC Press, Boca Raton, FL.

Wraith, J.M., and D. Or. 1999. Temperature effects on soil bulk dielectric permittivity measured by time domain reflectometry: Experimental evidence and hypothesis development. Water Resour. Res. 35:361–369.